

Article

Roughness Scaling Extraction Accelerated by Dichotomy-Binary Strategy and Its Application to Milling Vibration Signal

Feng Feng ¹, Meng Yuan ¹, Yousheng Xia ¹, Haoming Xu ¹, Pingfa Feng ^{1,2,*} and Xinghui Li ^{1,3,*}

¹ Division of Advanced Manufacturing, Shenzhen International Graduate School, Tsinghua University, Shenzhen 518055, China; feng.feng@sz.tsinghua.edu.cn (F.F.); ym20@mails.tsinghua.edu.cn (M.Y.); xiays18@mails.tsinghua.edu.cn (Y.X.); xhm19@mails.tsinghua.edu.cn (H.X.)

² Department of Mechanical Engineering, Tsinghua University, Beijing 100084, China

³ Tsinghua-Berkeley Shenzhen Institute, Tsinghua University, Shenzhen 518055, China

* Correspondence: feng.pingfa@sz.tsinghua.edu.cn (P.F.); li.xinghui@sz.tsinghua.edu.cn (X.L.)

Abstract: Fractal algorithms for signal analysis are developed from geometric fractals and can be used to describe various complex signals in nature. A roughness scaling extraction algorithm with first-order flattening (RSE-f1) was shown in our previous studies to have a high accuracy, strong noise resistance, and a unique capacity to recognize the complexity of non-fractals that are common in signals. In this study, its disadvantage of a long calculation duration was addressed by using a dichotomy-binary strategy. The accelerated RSE-f1 algorithm (A-RSE-f1) retains the three above-mentioned advantages of the original algorithm according to theoretical analysis and artificial signal testing, while its calculation speed is significantly accelerated by 13 fold, which also makes it faster than the typical Higuchi algorithm. Afterwards, the vibration signals of the milling process are analyzed using the A-RSE-f1 algorithm, demonstrating the ability to distinguish different machining statuses (idle, stable, and chatter) effectively. The results of this study demonstrate that the RSE algorithm has been improved to meet the requirements of practical engineering with both a fast speed and a high performance.

Keywords: roughness scaling extraction; fractal dimension; accelerated algorithm; Weierstrass–Mandelbrot function; milling vibration signal

MSC: 37M10



Citation: Feng, F.; Yuan, M.; Xia, Y.; Xu, H.; Feng, P.; Li, X. Roughness Scaling Extraction Accelerated by Dichotomy-Binary Strategy and Its Application to Milling Vibration Signal. *Mathematics* **2022**, *10*, 1105. <https://doi.org/10.3390/math10071105>

Academic Editors: Camelia Petrescu and Valeriu David

Received: 25 February 2022

Accepted: 28 March 2022

Published: 29 March 2022

Publisher's Note: MDPI stays neutral with regard to jurisdictional claims in published maps and institutional affiliations.



Copyright: © 2022 by the authors. Licensee MDPI, Basel, Switzerland. This article is an open access article distributed under the terms and conditions of the Creative Commons Attribution (CC BY) license (<https://creativecommons.org/licenses/by/4.0/>).

1. Introduction

Pioneered by the mathematician Mandelbrot [1,2], fractal geometry was established to investigate the morphological characteristics of filling space in the form of non-integer dimensions. Early studies have revealed that many features in nature have fractal characteristics, so fractal geometry is widely applied to a large variety of research areas, such as the influence of the fractal features of transects across vegetation on the arthropods living on its surface [3], the relationship between biological size and physiological function [4], and observations of the large-scale structure of the universe [5]. Follow-up studies found that fractals not only existed in features of nature, but also in various signals such as physiological electrical signals [6].

Fractal dimension (FD) is often used to measure the degree of geometric irregularity. Generally, the higher the complexity of the signal, the larger the corresponding FD value [7]. Therefore, many scholars have introduced FD into the research of signal processing in the medical field, such as electroencephalograms (EEG) [8] and electrocardiograms (ECG) [9–12], and have made remarkable achievements.

In recent years, signal fractals have been extended to the field of mechanical processing, such as the fractal characteristics of ultrasonic echoes and their application to nondestructive testing [13], the multifractal characteristics of ball mill dynamics [14], and the application

of vibration signal multifractals in fault diagnosis [15]. As a typical nonlinear signal, mechanical vibration has obvious fractal characteristics, and the complexity of the signal is closely related to the vibration state of the machine tool. Therefore, the fractal analysis of signals is also used to judge the machining status of machine tools. Ji et al. [16,17] proposed a multi-indicator chatter prediction method combining **FD**, power spectral entropy, and standard deviation. Zhuo et al. [18] identified chatter by calculating the **FD** of acceleration signals in thin-wall blade side milling. Chen et al. [19] proposed a multifractal method for chatter detection in milling processes. It can be seen that the application of **FD** in the field of manufacturing has been recognized.

There are various algorithms for calculating **FD**, including the box-counting (BC) algorithm [20], the Katz algorithm [21], and the Higuchi algorithm [22]. The Higuchi and box-counting algorithms have been widely used due to their practical applicabilities and fast speed [23–26]. In our previous study, a roughness scaling extraction (RSE) algorithm was proposed [27,28], and it has a higher accuracy and anti-noise performance compared with other traditional algorithms. The RSE algorithm can identify non-fractal features in signals [29], which is an ability that traditional fractal algorithms do not have. The RSE algorithm is based on the exponential relationship between scale (L) and root-mean-squared roughness (R_q), as shown in Equation (1). Firstly, Equation (2) is used to calculate the roughness values at each scale (L_i, R_{qi}), where $i = 1, 2, \dots, n$ represents the serial number of the data point, and \bar{y} represents the average of $y_i, \bar{y} = \frac{\sum_{i=1}^n y_i}{n}$, and then to obtain the dimension value D through Equation (3). $L = [L_1, L_2, \dots, L_p]$ represents the signal length at different scales, as well as the number of signal points ($L_i = [L_{i-1} \times \delta]$, δ represents the scaling ratio).

$$R_q = AL^{2-D} \tag{1}$$

$$R_q = \sqrt{\frac{\sum_{i=1}^n (y_i - \bar{y})^2}{n}} \tag{2}$$

$$\log R_q = (2 - D) \log L + \log A \tag{3}$$

The key procedure of the RSE algorithm is the flattening modification of sub-sequences that are segmented out of the concerned signal. The RSE algorithm with first-order flattening (RSE-f1) is the most accurate for fractal signals. First-order flattening refers to first-order polynomial fitting of the sub-sequences, as shown in Equation (4), where the expressions of a, b , and x_i are shown in Equation (5). The sequence of the RSE-f1 algorithm consists of the elements m_i calculated by Equation (6).

$$\hat{y}_i = b + ax_i \tag{4}$$

$$a = \frac{\sum_{i=1}^n x_i y_i - n \bar{x} \bar{y}}{\sum_{i=1}^n x_i^2 - n \bar{x}^2}; b = \bar{y} - a \bar{x}; x_i = i \tag{5}$$

$$m_i = y_i - \hat{y}_i \tag{6}$$

However, the disadvantage of the RSE algorithm is that calculations are time-intensive, which limits its application in practical engineering. Considering that the on-line recognition of the machining status of machine tools requires a fast response speed, the RSE algorithm needs to be accelerated to reflect the signal characteristics in a short delay of calculation. Therefore, an accelerated RSE-f1 (A-RSE-f1) algorithm based on a dichotomy and binary strategy is proposed in this paper. Based on theoretical analysis and artificial fractal signal testing, the A-RSE-f1 algorithm is much faster than the original RSE-f1 and the Higuchi algorithm, and it retains the high anti-noise performance of the RSE-f1 algorithm. Experimental results demonstrated that the A-RSE-f1 algorithm could distinguish the different machining statuses effectively of machining tools. In addition, the relationship between roughness and scale of the A-RSE-f1 algorithm is equivalent to that of the RSE-f1. Thus, the improvement does not change the fractal calculation principle of the algorithm.

2. Methods and Samples

2.1. Improvement of the RSE Algorithm

Specifically, the large scale sequence is divided into two small scale sequences, and the small scale sequence is divided successively until each subsequence contains only one element. In this way, it is guaranteed that sub-sequences at different scales do not overlap with each other and that the set of sub-sequences only covers the signal sequence, thus ensuring the calculation accuracy. It also adaptively changes the summation times of subsequence roughness according to the scale, which greatly improves the operation speed of the algorithm. As the formula and code of RSE-f0 are relatively simple, it is possible to find the core reason why the RSE algorithm requires a long time, so a dichotomy strategy was first used to preliminarily improve RSE-f0. In order to improve the accuracy of A-RSE-f0, it needs to carry out first-order flattening and realize random δ through a binary strategy, so as to obtain A-RSE-f1.

2.1.1. Accelerated RSE-f0 Algorithm

In order to accelerate the RSE algorithm, it must be clear what is taking the longest time in the program. Therefore, the pseudocode of the RSE algorithm without flattening (RSE-f0) can be written based on the above equations, as shown in Algorithm 1, where $stepN$ represents the number of subsequences of different lengths, and $subdata_i, R_q(m)_i$ represent the subsequence and roughness extracted for the i -th time at a certain scale, respectively. As the roughness of the small scale subsequence varies greatly in different positions of the signal sequence, it needs to be solved many times and then averaged, as shown in Lines 4 to 6 of the pseudocode. In order to ensure sufficient representativeness of the calculated roughness and a certain computational efficiency of the RSE-f0 algorithm, the roughness values of the 50 randomly selected sub-sequences are averaged as the final roughness value corresponding to the scale. However, it is this part of the operation that still greatly increases the time cost of the RSE-f0 algorithm. According to statistics, the 4~6 lines of the pseudocode account for 99% of the calculation duration of the algorithm. It is understood that, when the sub-sequence scale is large, many of the 50 randomly selected sub-sequences can overlap, and when the sub-sequence scale is small, it is difficult to completely cover the signal by randomly selecting positions. Therefore, to accelerate the RSE-f0 algorithm, calculating the roughness adaptively while covering the entire signal is key.

Algorithm 1 RSE-f0 algorithm

Input: $data$: signal data; δ : scaling ratio; $minpixle$: the number of elements of the; smallest scale; $repeat_{num}$: the calculating times of the roughness of the same scale

Output: D : the dimension value of the signal

```

1:  $stepN \leftarrow \lfloor \frac{\log(\frac{minpixle}{\delta})}{\log \delta} \rfloor$ 
2:  $L \leftarrow N \times \delta^{[0 \text{ to } stepN-1 \text{ do}]}, R_q(1)$ 
3: for each  $m \in [2, stepN]$  do
4:   for each  $i \in [1, repeat_{num}]$  do
5:      $subdata_i, R_q(m)_i$ 
6:   end for
7:    $R_q(m) \leftarrow mean(R_q(m)_i)$ 
8: end for
9:  $D \leftarrow 2 - \frac{\log R_q}{\log L}$ 

```

Aiming at this improvement, a preliminary accelerated algorithm based on RSE-f0 is proposed with a scaling ratio of 0.5. First, the dichotomy method is employed, thus the calculation flow is reversed, i.e., the roughness values are obtained from large sub-sequences to small ones in the original RSE-f0, while those in the A-RSE-f0 are from small sub-sequences to large ones. As sketched in Figure 1, each element in the sequence can be

regarded as a cell, and the combination of adjacent elements yields the next cell, which had twice the element number of the previous one. By analogy, the set of sub-sequences at various scales can be obtained, and the sub-sequences have no overlaps, which also ensures the full coverage of the signal. Obviously, based on the dichotomy method, the calculation times of the large-scale subsequence are shorter, while the calculation times of the small-scale subsequence are longer. For example, there are two sub-sequences after one scaling ($L_1 = 0.5 \times L$), while there are $\frac{1}{0.5^n}$ sub-sequences of the n -th scaling ($L_n = 0.5^n \times L$), which conforms to the previous goal of adaptively extracting the number of sub-sequences.

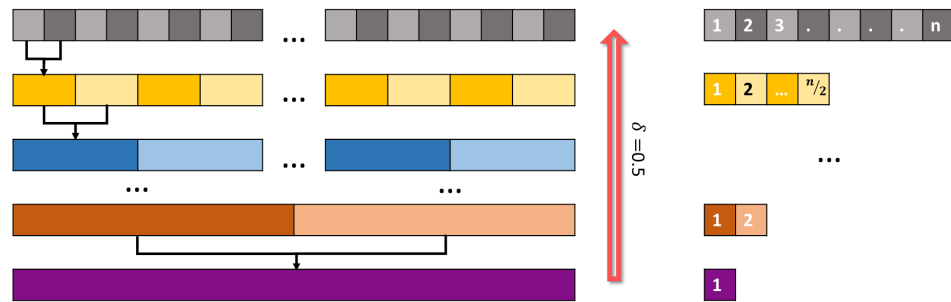


Figure 1. The schematic diagram of improving flow of A-RSE-f0 based on dichotomy method.

Further, the expression of the A-RSE-f0 algorithm is transformed, as shown in Equations (7) and (8). Equation (7) can be derived from Equation (1), where $A = \sum_{i=1}^n y_i^2$ and $B = \sum_{i=1}^n y_i$, thus obtaining Equation (8). The problem is then transformed into the construction of A and B matrices containing all scales by using the above dichotomy flow.

$$R_q^2 = \frac{\sum_{i=1}^n y_i^2}{n} - \left(\frac{\sum_{i=1}^n y_i}{n}\right)^2 \tag{7}$$

$$R_q^2 = \frac{A}{n} - \left(\frac{B}{n}\right)^2 \tag{8}$$

2.1.2. The Accelerated RSE-f1 Algorithm

The next aim of this study is to improve the RSE algorithm with first-order flattening (RSE-f1), whose accuracy is the highest [27]. The improved method based on the dichotomy idea can be extended to RSE-f1 as follows. Similar to that of A-RSE-f0, the expression of the A-RSE-f1 algorithm is also transformed. Equation (9) can be derived based on Equations (1) and (6). In Equation (9), $A = \sum_{i=1}^n y_i^2$, $C = \sum_{i=1}^n x_i y_i$ and $B = \sum_{i=1}^n y_i$ are set to obtain Equation (10). In this way, the problem is transformed into the construction of A, B, and C matrices containing various scales, and the solution of the intermediate parameters a and b. Thus, an A-RSE-f1 algorithm with $\delta = 0.5$ is obtained.

$$R_q^2 = \frac{\sum_{i=1}^n y_i^2 - a \sum_{i=1}^n x_i y_i - b \sum_{i=1}^n y_i}{n} \tag{9}$$

$$R_q^2 = \frac{A - aC - bB}{n} \tag{10}$$

However, in order to extend the scaling ratio of A-RSE-f1 to any value of δ to enhance its applicability, a binary strategy needs to be introduced. Specifically, extending to any δ is equivalent to the problem of extracting the subsequence between any two points in the signal sequence. Combined with Equations (9) and (10), the equivalent issue is how to quickly obtain the sum of the corresponding elements of the subsequence at any position.

For example, in order to obtain the sum from the first point to the P_{start} -th point in a sequence, the following operations can be conducted. Firstly, P_{start} is converted into binary numbers in the matrix constructed when $\delta = 0.5$ is used based on dichotomy. The i_{bin} -th bit in binary then corresponds to the i_{bin} -th row (a subsequence of length $2^{i_{bin}-1}$) and the $(P_{start} \gg (i_{bin} - 1))$ column element of the matrix, where \gg represents the

right-shift operation in binary. The sum of all elements of the matrix corresponding to 1 in the binary number is the sum of the target sequence. As shown in Figure 2, if $P_{start} = 7$, it can be written as 111 after it is converted to binary. Its first digit (from right to left) is 1, corresponding to the first row and seventh column of the matrix. The second digit is also 1, corresponding to the second row and third column of the matrix. The third digit is also 1, corresponding to the third row and the first column of the matrix. The above three elements in the matrix are then summed, as shown in Equation (11). The problem is then transformed from a sum of seven elements to a sum of three elements, effectively reducing the time of summation and thus reducing the calculation duration. If the sum of elements between any two points is required, the sum from the first point to the P_{end} -th point $SUM_{P_{end}}$ and the sum from the first point to the P_{start} -th point $SUM_{P_{start}}$ can be obtained by the above algorithm, respectively, and the sum from the P_{start} -th point to the P_{end} -th point can then be obtained by $SUM_{P_{end}} - SUM_{P_{start}}$, as shown in Equation (12). Understandably, the overlapping elements cancel each other out while they are subtracted, resulting in a sum of the target elements, as shown in Figure 3.

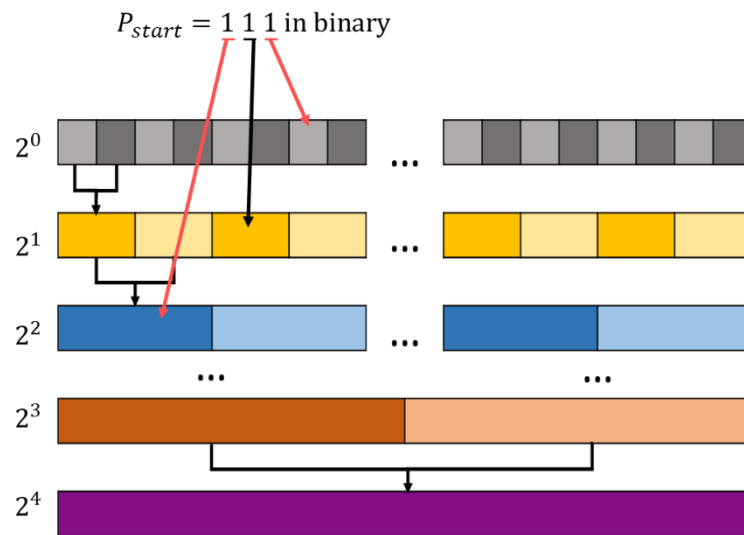


Figure 2. A diagram of the sum from the first point to the P_{start} -th ($=7$) point of the sequence in binary, which is employed for A-RSE-f1.

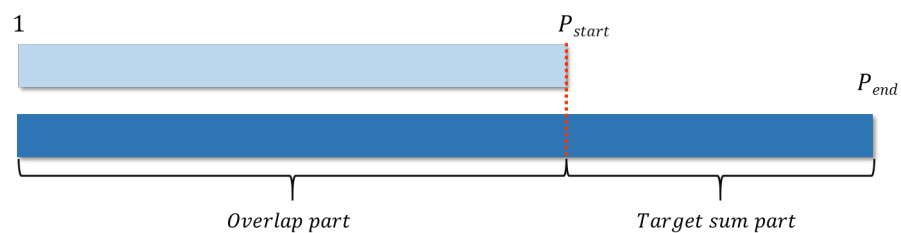


Figure 3. Diagram of summation of subsequence from P_{start} to P_{end} .

To summarize the above methods in a mathematical language, auxiliary matrices A, B, and C are denoted as $TEMP$, as shown in Equation (11), where $TEMP(i_{bin}, P \gg (i_{bin} - 1))$ represents the element of the $(P \gg (i_{bin} - 1))$ column of the i_{bin} row of the auxiliary matrix. In Equation (13), $\zeta(i)$ represents a two-valued function that returns 1 when the i_{bin} bit of the binary number is 1, and 0 when the i_{bin} bit is 0. After converting P_{start} into binary (P_{bin}), traverse all the elements in the auxiliary matrix corresponding to 1 contained in P_{bin} , and these values are then summed. Therefore, the number of summations in Equation (11) depends on the number of 1s contained in the P_{bin} .

$$SUM_{P_{start}} = \sum TEMP(i_{bin}, P_{start} \gg (i - 1))\zeta(i) \tag{11}$$

$$SUM = SUM_{P_{end}} - SUM_{P_{start}} \tag{12}$$

$$\zeta(i) = \begin{cases} 0 & \text{if the } i\text{-th bit of } P \text{ in binary is } 0 \\ 1 & \text{if the } i\text{-th bit of } P \text{ in binary is } 1 \end{cases} \tag{13}$$

In such a manner, the A-RSE-f1 algorithm achieved the aim of being adaptive and providing full coverage in the sub-sequence extraction based on the idea of a dichotomy so as to avoid repeated calculations caused by random selections with fixed times. The binary strategy was then used to reduce the summation times, thus further accelerating the summation process of corresponding elements. Compared with the RSE-f1 algorithm, the improvements of the A-RSE-f1 algorithm are based on equivalent operations via the dichotomy-binary strategy and thus do not change its principle, maintaining the accuracy of calculation.

2.2. Samples

2.2.1. Artificial Fractal and Non-Fractal Signals

As the true value of D cannot be obtained in prior for the actual fractal features, it is difficult to evaluate the advantages and disadvantages of different fractal algorithms by using signals from nature. Therefore, using a fractal function to generate ideal fractal signals or surfaces is an important approach to evaluate the performance of different fractal algorithms. The fractal function has the property of being continuous everywhere, but not differentiable [29]. The functions commonly used for generating fractal signals include the Weierstrass–Mandelbrot (W-M) function [30,31], the Monte Carlo function [32], the Takagi function [33], and the Brownian motion function [34]. Among them, the W-M function is widely used in the field of fractal analysis [35–39]. Moreover, the abnormal implementation of the W-M function enables it to generate non-fractal profiles or surfaces [29]. According to our previous research, actual signals or surfaces in nature also have non-fractal features, while traditional fractal algorithms (including Higuchi and box-counting) cannot recognize the complexity of non-fractal characteristics. Therefore, in this study, the W-M function is used to generate both fractal and non-fractal signals, so as to evaluate the performances of different algorithms.

The mathematical expression of the W-M function is shown in Equation (14), where D is the ideal *Dimension* value of the generated signals; γ is the density of frequencies in the signal; M is the number of superposed ridges; ϕ_n is a random phase shift; and n is a frequency index. Fifty groups of fractal signals for each D , ranging from 0.1 to 2 with an interval of 0.1, were generated by the W-M function. Relevant pictures can be seen in the previous research [27]. It can be seen that, with the increase in the D value, the complexity of the curve is higher and the fluctuation of it is more severe.

$$W(x) = \sum_{n=0}^M \gamma^{(D-2)n} [\cos\phi_n - \cos(\gamma^n x + \phi_n)] \tag{14}$$

2.2.2. Milling Vibration Signals

In order to apply the A-RSE-f1 algorithm in practical engineering, it is not sufficient to test its performance only with the generated ideal fractal signals. It also needs to use real machining signals for verification purposes. Milling is one of the most important machining technologies in the field of manufacturing. However, the severe vibration of machine tools usually leads to the deterioration of workpiece surface quality, thus reducing work efficiency. Therefore, many methods to predict and suppress chatter have been proposed, including the establishment of a stability lobe diagram (SLD) [40], a cutting dynamics model [41], and online monitoring [42,43]. Recognizing the signal characteristics of machine tools is an important on-line monitoring method for preventing chatter [44–48]. For industries, an acceleration signal is generally recommended [49]. Therefore, the application effect of the A-RSE-f1 algorithm in practical engineering was verified by milling acceleration signals. The experimental equipment and data analysis are illustrated in Figure 4.

The machining signals used in this study were the acceleration signals of the machine tool spindle collected by the experimental equipment. The data acquisition process was carried out using an accelerometer fixed on the spindle of the machine tool. The data of the sensor were collected using the Simens LMS TestLab 17 software and finally transmitted to the computer. The vertical machining center was the EUMA DU810, and the accelerometer used was a PCB piezoelectric triaxial vibration sensor. The partial enlargement of the workbench and the workpiece surface obtained by two machining statuses (stable and chatter) are shown in Figure 4b. The data acquisition equipment was an LMSSCADASIII multi-channel data acquisition front end, as shown in Figure 4c.

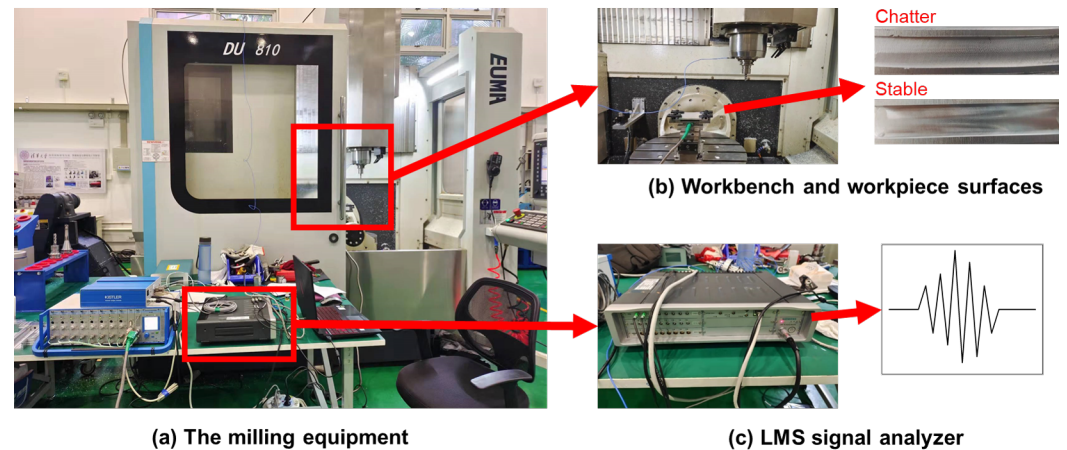


Figure 4. The final assembly of: (a) the milling equipment, (b) workbench and workpiece surfaces, and (c) LMS signal analyzer.

3. Results and Discussion

3.1. Ideal Fractal Signals Testing

In order to test the improvement effect of this study, the original RSE-f1, A-RSE-f1, Higuchi, and BC algorithms were used to calculate 20×50 artificial signals generated by the above W-M function. In this study, δ of the A-RSE-f1 has been extended to any value. Therefore, in order to evaluate the improved algorithm comparatively, the δ values of both A-RSE-f1 and RSE-f1 were set as $\delta = 0.85$.

Firstly, the calculated dimension (D_c) values by RSE-f1, A-RSE-f1, Higuchi, and BC algorithms were compared with the ideal dimension (D_i) values, as plotted in Figure 5. Obviously, when D value is less than 1, the calculation results of the Higuchi and BC algorithms are close to 1, while both the RSE-f1 and A-RSE-f1 algorithms could effectively approximate the D_i value. When the D value is above 1, the curves of RSE-f1, A-RSE-f1, and Higuchi are very close to D_i , but there is significant deviation in the BC curve.

To quantify the deviation of the above four algorithms, the logarithmic coordinate plot of the mean relative error (MRE) under different D_i were summarized, as shown in Figure 6. It can be seen that, when D_i is less than 1, the MRE values of RSE-f1 and A-RSE-f1 are much smaller than those of the Higuchi and BC algorithms, consistent with the results in Figure 5. These two traditional algorithms are completely invalid in the non-fractal region. When D_i is greater than 1, the MRE values of BC are generally greater than those of RSE-f1 and A-RSE-f1, while the Higuchi algorithm has a high accuracy when D_i is close to 2. It can also be observed in Figure 5 that the D_c values of the Higuchi algorithm are all larger than D_i , which is consistent with what is shown in Figure 6. By contrast, RSE-f1 and A-RSE-f1 both have high computational accuracy even in the non-fractal region, and their MREs are below 2% in the fractal region. Therefore, RSE-f1 and A-RSE-f1 are applicable to a wider range than are the other algorithms in terms of analyzing the signals of fractal and non-fractal regions.

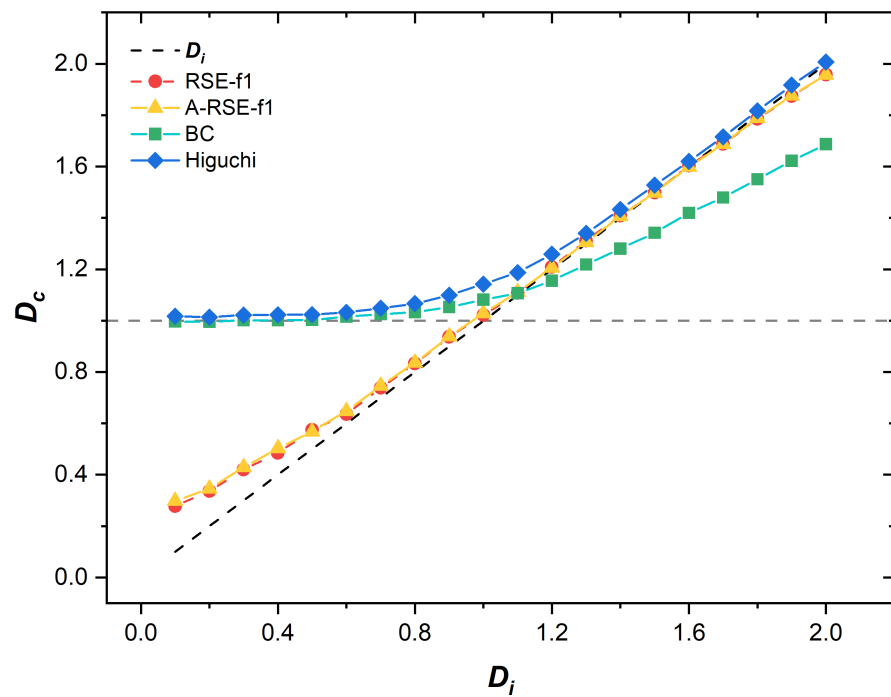


Figure 5. Comparison of the ideal dimension (D_i) and the calculated dimension (D_c) by RSE-f1, A-RSE-f1 Higuchi, and BC algorithms.

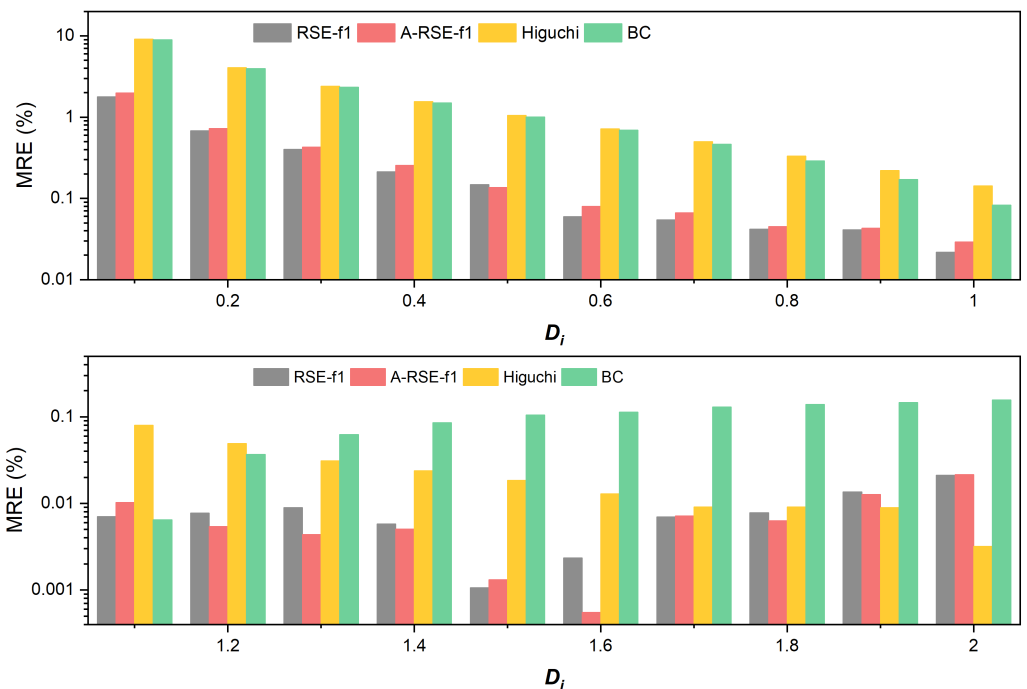


Figure 6. The logarithmic coordinate plot of the mean relative error (MRE) of RSE-f1, A-RSE-f1, Higuchi, and BC algorithms under different D_i values.

A major advantage of A-RSE-f1 compared with RSE-f1 is that its calculation speed is greatly accelerated. Figure 7 shows the single running duration (SRD) and standard deviation (STD) of the RSE-f1, A-RSE-f1, Higuchi, and BC algorithms. The calculation speed of A-RSE-f1 is significantly higher than that of the RSE-f1 algorithm by about 13 folds, and is also faster than that of the Higuchi algorithm, indicating that A-RSE-f1 based on a dichotomy and binary strategy has an advantage in terms of calculation speed. The

A-RSE-f1 algorithm only needs 7.8×10^{-3} s for a single running, which meets the practical engineering requirements. However, the RSE algorithm has the disadvantage of a large fluctuation in the results. As shown in Figure 7, the STD values of both RSE algorithms are higher than those of the Higuchi and BC algorithms, so multiple measurements are needed to eliminate such fluctuation.

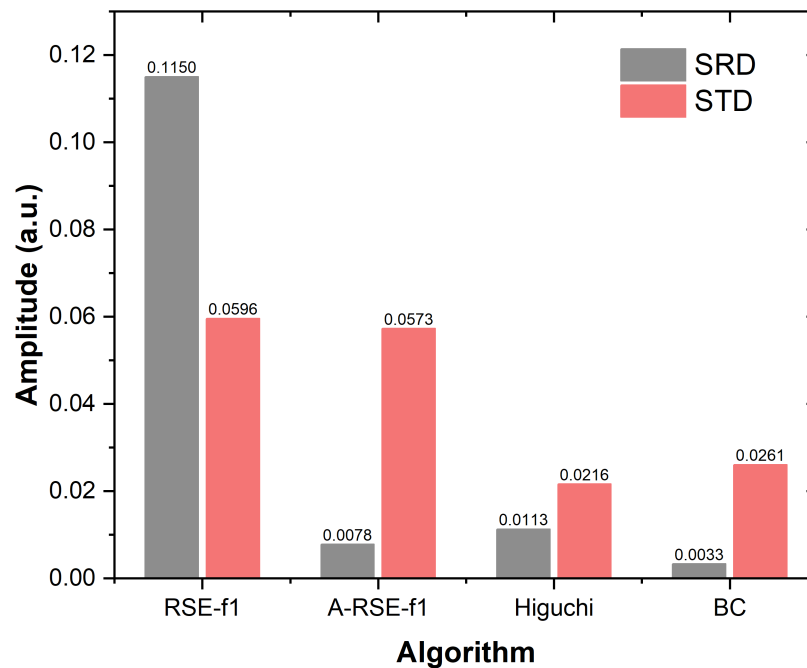


Figure 7. The single running Duration (SRD) and standard deviation (STD) of the RSE-f1, A-RSE-f1, Higuchi, and BC algorithms.

In essence, the collected signals in reality are always mixed with noise, which will reduce the efficiency of the calculations [50], so the algorithm must have an ability to resist noise. Therefore, the anti-noise performance of the RSE-f1, A-RSE-f1, Higuchi, and BC algorithms were also compared. The signal–noise ratios (SNRs) used in this study were 0, 5, . . . , 50 dB. As shown in Figure 8, the MRE values of the artificial signals after adding noise were calculated by the four algorithms. It can be seen that, when the D_i and SNR are both small, the anti-noise performance of all algorithms is low, because noise dominates the characteristics of the signals, and the D_c values are all close to 2, leading to large calculation errors. With the increase in SNR, the MRE values of all algorithms except BC gradually decrease, because the proportion of noise decreases. The BC algorithm shows an opposite trend in many cases. As indicated in Figure 5, the D_c values of the BC algorithm are low, and the deviation becomes larger with the increase in D_i . When D_i is large, noise plays a role in compensation, making BC more accurate, which is an interesting result. Globally, the MREs of the RSE-f1 and A-RSE-f1 algorithms are lower than those of the Higuchi and BC algorithms, demonstrating that the RSE-f1 algorithm has a strong anti-noise property, and its accelerated version, A-RSE-f1, retains this property.

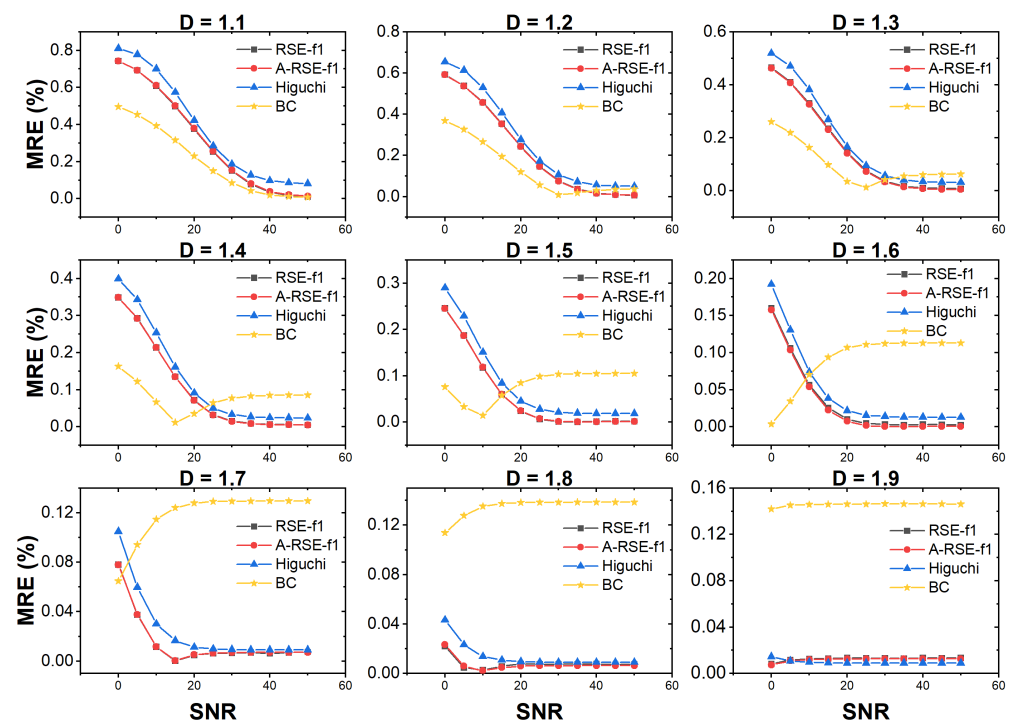


Figure 8. The comparison of anti-noise performances of RSE-f1, A-RSE-f1 Higuchi, and BC algorithms under different D_i and signal-noise-ratio (SNR) values.

3.2. Chatter Recognition in Milling

As shown in Figures 9 and 10, the typical acceleration signals of stable and chatter statuses are significantly different. The above signals were denoised by a five-order wavelet method, and the two sets of signals were calculated by the RSE-f1, A-RSE-f1, Higuchi, and BC algorithms. The length of the stable signal in Figure 9 is 30 s, of which 5–25 s is under a stable status of machining. The length of the chatter signal in Figure 10 is 13.5 s, of which 3.5–12 s is under a chatter status of machining. It can be seen that the calculation results of the RSE-f1, A-RSE-f1, and Higuchi algorithms vary accordingly, along with the operations and statuses of the milling process. The D values of stable milling are less than 1.4, and those of chatter milling are greater than 1.9. However, the D values calculated by the BC algorithm are about 1.5 in the stable milling and 1.7 in the chatter milling. The BC algorithm might not distinguish the acceleration signals of stable and chatter milling effectively and may not be suitable for the chatter recognition of acceleration signals. In addition, the D values of the idling status calculated by RSE-f1 and A-RSE-f1 are generally less than 1, indicating the non-fractal nature of the signals under such conditions. The Higuchi and BC algorithms cannot recognize non-fractal features, so their chatter recognition abilities are weaker. In particular, the D values of acceleration signals calculated by the Higuchi method in the idling status are basically the same as those in stable machining, as shown in Figure 9.

Vibration interference is an important factor restricting the development of computer numerical control (CNC) machine tool technology, including free vibration, forced vibration, and self-excited vibration. Chatter is a kind of complex, self-excited vibration, which is also the most serious form of vibration affecting the processing system. The real-time monitoring and recognition method can detect the status change of machine tools in time, so as to enable the suppression of the harm of chatter to workpiece and machine tools. However, the developments of chatter monitoring and suppression require recognition algorithms with both high accuracy and speed.

In order to further evaluate the application effect of A-RSE-f1 in signal recognition, 40 groups of milling acceleration signals (20 stable signals and 20 chatter signals) are

identified by the above four algorithms. The calculation durations for 40 groups of signals are listed in Table 1. The calculation durations are ordered as follows: RSE-f1 > Higuchi > A-RSE-f1 > BC. It can be seen that A-RSE-f1 is a significant improvement over RSE-f1 in terms of calculation speed and can thus meet the computing requirements of practical engineering applications.

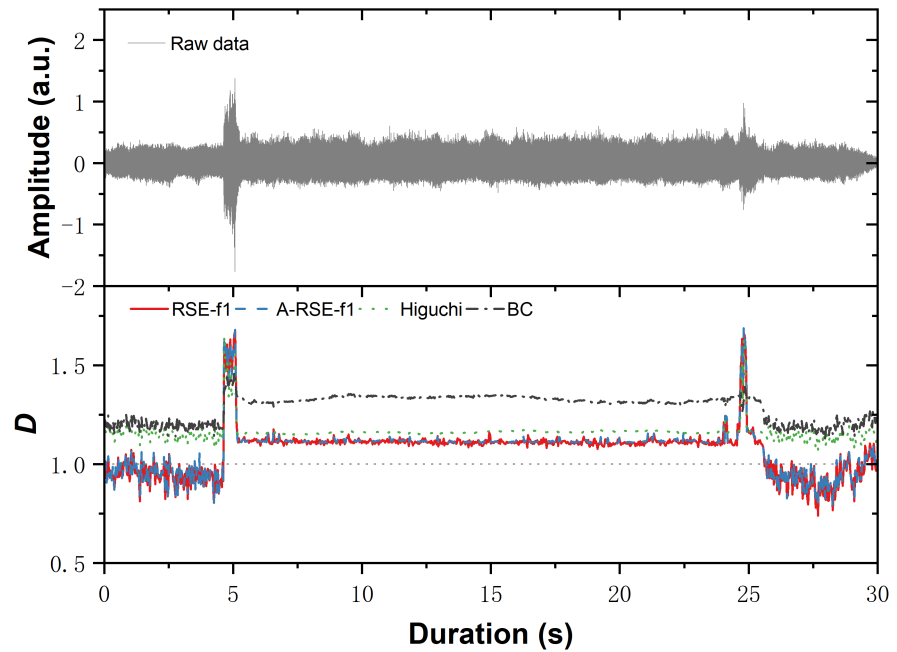


Figure 9. The acceleration signals of stable milling and D values of signal calculated by RSE-f1, A-RSE-f1, Higuchi, and BC algorithms.

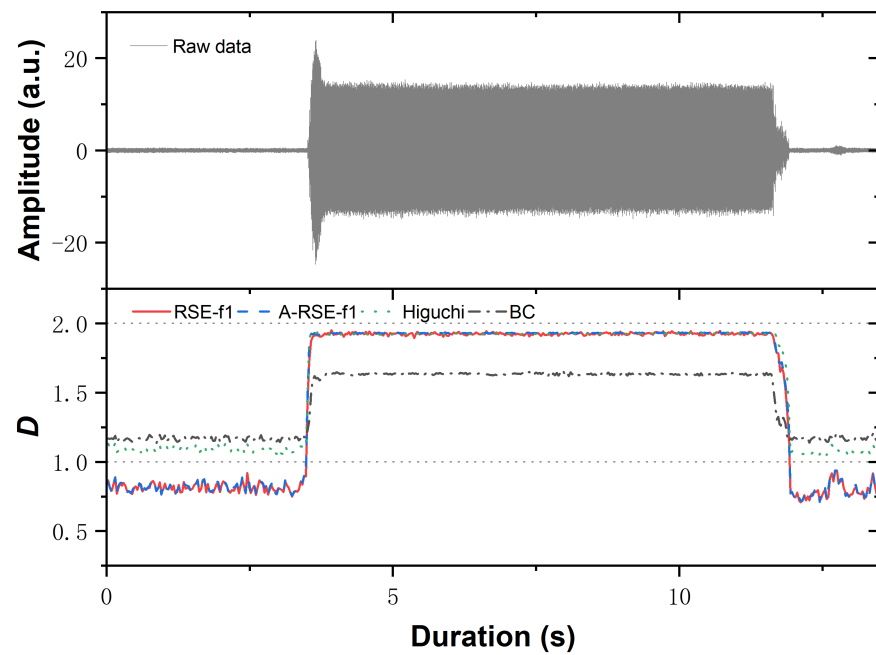


Figure 10. The acceleration signals of chatter status and D values of signal calculated by RSE-f1, A-RSE-f1, Higuchi, and BC algorithms.

Table 1. The calculation durations of RSE-f1, A-RSE-f1, Higuchi, and BC algorithms to process all 40 sets of vibration signals.

| Algorithm | RSE-f1 | A-RSE-f1 | Higuchi | BC |
|--------------|--------|----------|---------|-------|
| Duration (s) | 2439 | 157.7 | 249.1 | 65.41 |

Machining statuses can be idling, stable, or chatter. In order to ensure the consistent proportion of data in various machining statuses and the representativeness of signal samples, 100 D values were randomly selected from the results of 20 chatter signals in the idling stage and the machining stage and of 20 stable signals in the signal machining stage, respectively, so each machining status calculated by each algorithm has 2000 data points. The above data are plotted in Figure 11 and form the histogram of the D -value distribution of 40 signals at different statuses calculated by the four algorithms. Obviously, the results of the RSE-f1, A-RSE-f1, and Higuchi algorithms have less overlap in the stable and chatter parts than the BC algorithm, indicating that these three algorithms can better identify the chatter characteristics of milling acceleration signals. As for idling and stable statuses, it can be seen that the RSE-f1 and A-RSE-f1 algorithms have the least overlap. As the acceleration signal of the machine tool spindle is relatively simple during idling, it embodies more non-fractal characteristics. The calculated D values of RSE-f1 and A-RSE-f1 are basically less than 1, which is consistent with the performance of actual machining, indicating that these two algorithms are applicable to a wider range. However, the Higuchi and BC algorithms cannot recognize non-fractal signals, so the calculation results of the idling part will partially overlap with stable processing.

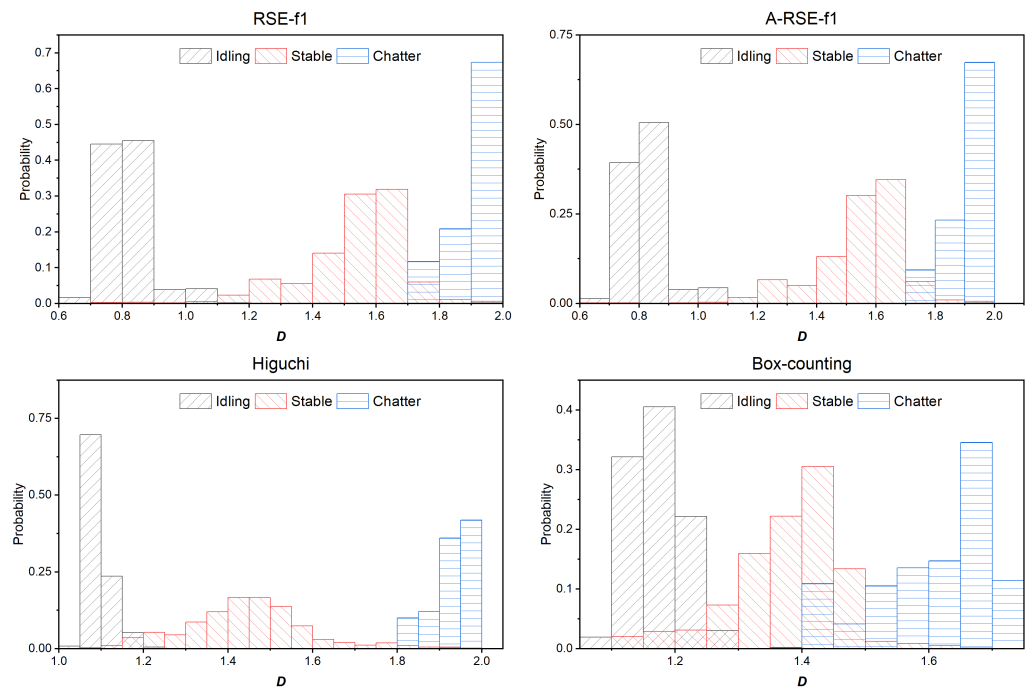


Figure 11. Histogram of D values distribution of 40 signals at different statuses calculated by RSE-f1, A-RSE-f1, Higuchi, and BC algorithms.

The A-RSE-f1 algorithm is significantly faster than the RSE-f1 algorithm and even faster than the Higuchi algorithm. Moreover, A-RSE-f1 can recognize non-fractal features, so the machining status of idling, stable, and chatter can be distinguished significantly according to the acceleration signal of the spindle of the machine tool. Although the calculation speed of the BC algorithm is faster, its accuracy and noise resistance are weak, and it is difficult to distinguish different machining statuses effectively. Therefore, the

A-RSE-f1 algorithm has the best comprehensive performance with a fast calculation speed, a high accuracy, strong noise resistance, and a wide application range, and can distinguish different processing statuses effectively.

3.3. Effects of Cutting Parameters

The establishment of a milling stability lobe diagram [51] is a method used to predict machining status, and the occurrence of chatter can be avoided by inducing stable cutting parameters under certain working conditions. Therefore, the selection of machining parameters is closely related to machining status and vibration signal. The influence of processing parameters on signal dimension will be explored below.

The experimental equipment is described in Section 2.2.2. The workpieces are 7075 120 mm × 120 mm × 10 mm aluminum alloy square plates, and the cutting tool is a tungsten steel 3-edge milling cutter with A diameter of 10 mm. A total of 36 groups of machining parameters, including changes in feed, cut depth, and speed, are summarized in Table 2. Fifty windows were randomly selected for each signal (each window contains 1024 data points), and 50 *D* values were calculated and averaged. According to the above analysis, the calculation results of RSE-f1 and A-RSE-f1 are almost the same, while the calculation duration of RSE-f1 is much longer, so only the A-RSE-f1, Higuchi, and BC algorithms were used for calculation. The calculation results are illustrated in Figure 12.

Table 2. 36 groups of machining parameters with various feed, cut depth and speed values.

| No. | Speed (r/s) | Depth (10 ⁻³ m) | Feed (10 ⁻³ m/s) |
|-----|-------------|----------------------------|-----------------------------|
| 1 | | | 8.3 |
| 2 | | | 9.2 |
| 3 | 50.0 | 1.0 | 10.0 |
| ... | | | ... |
| 13 | | | 18.3 |
| 14 | | 0.5 | |
| 15 | | 0.7 | |
| 16 | 150.0 | 0.9 | 6.7 |
| ... | | ... | |
| 26 | | 2.9 | |
| 27 | 50.0 | | |
| 28 | 66.7 | | |
| 29 | 83.3 | 1.0 | 5.0 |
| ... | ... | | |
| 36 | 200.0 | | |

As shown in Figure 12a, the *D* values calculated by the A-RSE-f1 and Higuchi algorithms all increased with the increase in the feed, among which the results of A-RSE-f1 show a more obvious upward trend. The feed per tooth can be expressed as $F/(3S)$, where F (m/s) represents the feed speed, and S (r/s) stands for spindle speed. The experimental tool has three teeth. Under the condition of the same speed and cutting depth, the larger the feed per tooth, the more likely it is to cause chatter, resulting in a higher *D* in the acceleration signal of the spindle. As shown in Figure 12b, the *D* values calculated by the A-RSE-f1 and Higuchi algorithms drop significantly when the cutting depth range is 0.5~1.3 mm, indicating that the machine tool is prone to violent vibrations when the cutting depth is very small, consistent with the experimental phenomenon. When the cutting depth is greater than 1 mm, the *D* values of the acceleration signal are relatively stable, indicating that the cutting depth has little influence on the vibration of the machine tool within this range. However, a greater cutting depth can increase the cutting force of the tool, such that the tool can be more vulnerable to damage. As shown in Figure 12c, the *D* values calculated by the A-RSE-f1 and Higuchi algorithms generally show a downward trend along with the increase in spindle speed. This is similar to the situation in Figure 12a. As the spindle speed

increases, the feed per tooth decreases, so the possibility of chatter and the complexity of acceleration signal both decrease. However, a higher rotational speed can lead to a tool temperature that is too high, which becomes negative for machining. In addition, as shown in Figure 12, the calculation results of the BC algorithm are significantly different from those of the other algorithms, indicating that the BC algorithm is not sensitive to the changes of machining parameters, which further verifies that the BC algorithm is not suitable for the application to machining within the research scope of this study.

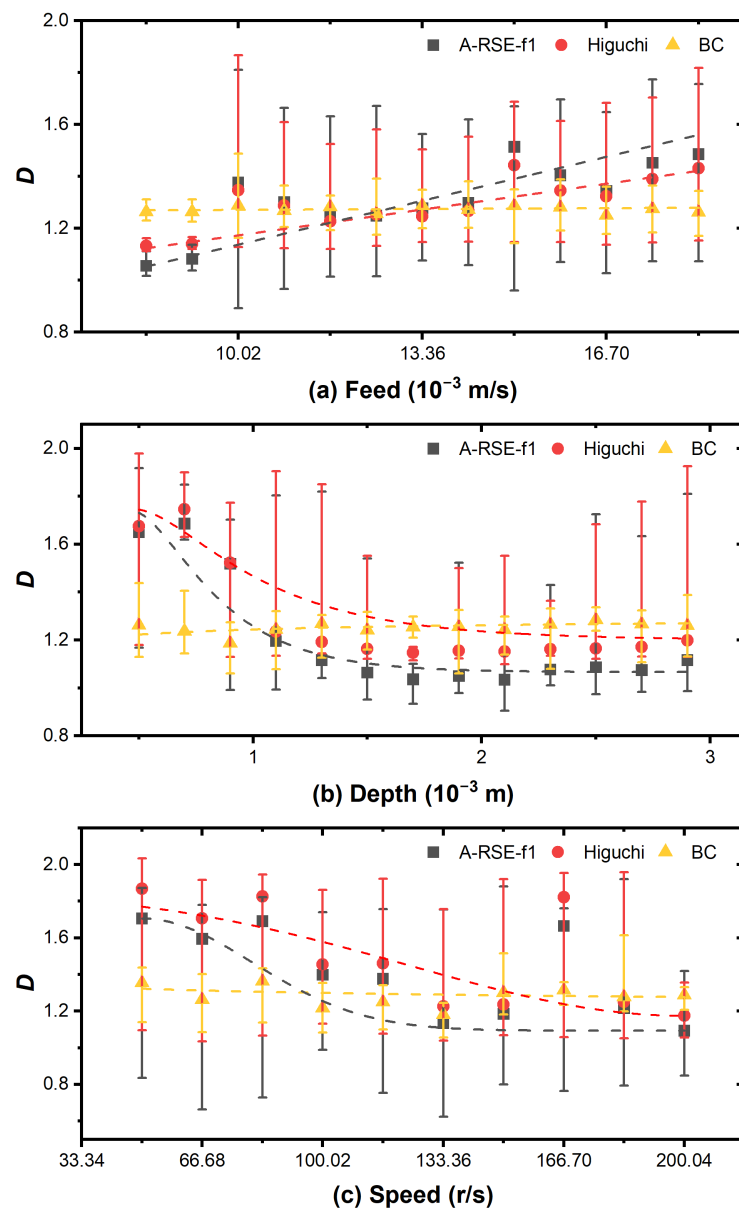


Figure 12. The calculation of D values of milling acceleration signal by A-RSE-f1, Higuchi, and BC algorithms, and the influences of: (a) feed, (b) cut depth, and (c) speed.

The variation range of the calculation results of the A-RSE-f1 algorithm is larger than the other two algorithms. This fact indicates that the A-RSE-f1 algorithm is more sensitive to the change in signal characteristics, and the algorithm can recognize more characteristics that the other algorithms cannot. In conclusion, under the working conditions of this experiment, a speed of 83.3~150 r/s, a cutting depth of more than 1 mm, and a small feed are more appropriate machining parameters. Furthermore, the influences of each parameter on the machining status are coupled, while the establishment of the SLD preliminarily

predicts the speed and cutting depth range of stable machining but ignores the influence of the feed [52,53]. This issue will be further investigated in our future work.

4. Conclusions

In this study, an accelerated RSE-f1 (with first-order flattening) algorithm, A-RSE-f1, is proposed. Based on the strategy of a dichotomy, the random selection of a fixed number of sub-sequences in the RSE-f1 algorithm is changed to be adaptive and provide full coverage of the signal, avoiding redundant calculations. The auxiliary matrices are constructed based on a binary strategy to reduce the time of summation and further accelerate the algorithm. The improvement effect of the A-RSE-f1 algorithm is tested using fractal ($D = 1\sim 2$) and non-fractal ($D = 0\sim 1$) signals generated by the W-M function, and the engineering application of the A-RSE-f1 algorithm is demonstrated using 40 milling acceleration signals (20 chatter signals and 20 stable signals) of the machine tool spindle. In addition, the effects of different machining parameters on the acceleration signals and the D values are discussed. It should be noted that, due to differences in applicable parameters and signal characteristics in various experimental conditions, the experimental results analyzed by the A-RSE-f1 algorithm above are only verified within the experimental condition of this study, and the feasibility of its utilization under other experimental conditions will be investigated in our future work. The specific conclusions are as follows:

1. A-RSE-f1 is proposed based on a dichotomy and binary strategy. The A-RSE-f1 algorithm not only has been shown to be more accurate than the Higuchi and BC algorithms, but also is much faster than the original RSE-f1 algorithm by about 13 folds and 1.5-fold faster than the Higuchi algorithm. In the range of accuracy allowed, the lower scaling ratio δ can further improve the operation speed.
2. Through the verification of 40 groups of milling acceleration signals, it is shown that the RSE-f1 and A-RSE-f1 algorithms can recognize the machining signals of different statuses and can be applied to the chatter recognition of machine tools. The A-RSE-f1 algorithm can also identify the non-fractal characteristics of machining signals, which can play an important role in further studies of the physical significance of signal characteristics.
3. The single running duration of $\delta = 0.85$ of the A-RSE-f1 algorithm is only 7.8×10^{-3} s. In the range of accuracy allowed, the lower scaling ratio δ can further improve the operation speed. Therefore, A-RSE-f1 is promising in that it can meet the application requirements of practical engineering and can be used for chatter recognition through the acceleration signals in milling.

Author Contributions: Conceptualization, F.F. and Y.X.; Data curation, M.Y.; Funding acquisition, P.F.; Investigation, F.F.; Methodology, X.L.; Project administration, P.F.; Software, Y.X. and H.X.; Supervision, X.L.; Validation, H.X.; Writing—original draft, F.F. and M.Y.; and Writing—review and editing, X.L. All authors have read and agreed to the present version of the manuscript.

Funding: This study was supported by National Natural Science Foundation of China under Grant No. 51875311, Guangdong Basic and Applied Basic Research Foundation under Grant No. 2020A1515011199, and Shenzhen Natural Science Foundation under Grant No. WDZC20200817152115001.

Institutional Review Board Statement: Not applicable.

Informed Consent Statement: Not applicable.

Data Availability Statement: The data presented in this study are available from the corresponding author with reasonable request. Moreover, the codes of analysis and simulation on fractal profiles and surfaces have been established, and the collaboration investigation by using them is welcome by the authors.

Acknowledgments: The authors would like to thank Shaozhu Xiao, Xiangsong Zhang, Binbin Liu, Shaocong Wang, Junlong Huang, Jun Li, Yousheng Xia, and Zengxian Ma of Tsinghua University for their contributions to fractal studies in our lab.

Conflicts of Interest: The authors declare no conflict of interest.

References

- Mandelbrot, B.B. Is nature fractal? *Science* **1998**, *279*, 783. [[CrossRef](#)]
- Mandelbrot, B.B.; Mandelbrot, B.B. *The Fractal Geometry of Nature*; WH Freeman: New York, NY, USA, 1982; Volume 1.
- Morse, D.R.; Lawton, J.; Dodson, M.; Williamson, M. Fractal dimension of vegetation and the distribution of arthropod body lengths. *Nature* **1985**, *314*, 731–733. [[CrossRef](#)]
- Williams, N. Biology: Fractal geometry gets the measure of life's scales. *Science* **1997**, *276*, 34. [[CrossRef](#)] [[PubMed](#)]
- Luo, X.; Schramm, D.N. Fractals and cosmological large-scale structure. *Science* **1992**, *256*, 513–515. [[CrossRef](#)] [[PubMed](#)]
- Namazi, H.; Ala, T.S. Decoding of simple and compound limb motor imagery movements by fractal analysis of electroencephalogram (eeg) signal. *Fractals* **2019**, *27*, 1950041. [[CrossRef](#)]
- Eke, A.; Herman, P.; Kocsis, L.; Kozak, L. Fractal characterization of complexity in temporal physiological signals. *Physiol. Meas.* **2002**, *23*, R1. [[CrossRef](#)]
- Akar, S.A.; Kara, S.; Latifoğlu, F.; Bilgic, V. Investigation of the noise effect on fractal dimension of eeg in schizophrenia patients using wavelet and ssa-based approaches. *Biomed. Signal Process. Control* **2015**, *18*, 42–48. [[CrossRef](#)]
- Raghav, S.; Mishra, A.K. Fractal feature based eeg arrhythmia classification. In Proceedings of the TENCON 2008—2008 IEEE Region 10 Conference, Hyderabad, India, 19–21 November 2008; pp. 1–5.
- Pina-Vega, R.P.; Valtierra-Rodriguez, M.; Perez-Ramirez, C.A.; Amezquita-Sanchez, J.P. Early prediction of sudden cardiac death using fractal dimension and eeg signals. *Fractals* **2021**, *29*, 2150077–2151052. [[CrossRef](#)]
- Marie, R.R.; Al Alfi, M.H. Identification of cardiac diseases from (eeg) signals based on fractal analysis. *Int. J. Comput. Technol.* **2014**, *13*, 4556–4565. [[CrossRef](#)]
- Sharma, V. Deterministic chaos and fractal complexity in the dynamics of cardiovascular behavior: Perspectives on a new frontier. *Open Cardiovasc. Med. J.* **2009**, *3*, 110. [[CrossRef](#)]
- Shoupeng, S.; Peiwen, Q. A fractal-dimension-based signal-processing technique and its use for nondestructive testing. *Russ. J. Nondestruct.* **2007**, *43*, 270–280. [[CrossRef](#)]
- Budroni, M.A.; Pilosu, V.; Delogu, F.; Rustici, M. Multifractal properties of ball milling dynamics. *Chaos Interdiscip. J. Nonlinear Sci.* **2014**, *24*, 023117. [[CrossRef](#)]
- Yu, Y.; Baoliang, L.; Jingshan, S.; Shixuan, Y. The application of vibration signal multi-fractal in fault diagnosis. In Proceedings of the 2010 Second International Conference on Future Networks, Sanya, China, 22–24 January 2010; pp. 164–167.
- Ji, Y.; Wang, X.; Liu, Z.; Yan, Z.; Jiao, L.; Wang, D.; Wang, J. Eemd-based online milling chatter detection by fractal dimension and power spectral entropy. *Int. J. Adv. Manuf. Technol.* **2017**, *92*, 1185–1200. [[CrossRef](#)]
- Ji, Y.; Wang, X.; Liu, Z.; Wang, H.; Jiao, L.; Wang, D.; Leng, S. Early milling chatter identification by improved empirical mode decomposition and multi-indicator synthetic evaluation. *J. Sound Vib.* **2018**, *433*, 138–159. [[CrossRef](#)]
- Zhuo, Y.; Jin, H.; Han, Z. Chatter identification in flank milling of thin-walled blade based on fractal dimension. *Procedia Manuf.* **2020**, *49*, 150–154. [[CrossRef](#)]
- Chen, Y.; Li, H.; Hou, L.; Bu, X.; Ye, S.; Chen, D. Chatter detection for milling using novel p-leader multifractal features. *J. Intell. Manuf.* **2020**, *33*, 1–15. [[CrossRef](#)]
- Liebovitch, L.S.; Toth, T. A fast algorithm to determine fractal dimensions by box counting. *Phys. Lett. A* **1989**, *141*, 386–390. [[CrossRef](#)]
- Katz, M.J. Fractals and the analysis of waveforms. *Comput. Biol. Med.* **1988**, *18*, 145–156. [[CrossRef](#)]
- Higuchi, T. Approach to an irregular time series on the basis of the fractal theory. *Phys. D Nonlinear Phenom.* **1988**, *31*, 277–283. [[CrossRef](#)]
- Kesić, S.; Spasić, S.Z. Application of higuchi's fractal dimension from basic to clinical neurophysiology: A review. *Comput. Methods Programs Biomed.* **2016**, *133*, 55–70. [[CrossRef](#)]
- Khoa, T.Q.D.; Ha, V.Q.; Toi, V.V. Higuchi fractal properties of onset epilepsy electroencephalogram. *Comput. Math. Methods Med.* **2012**, *2012*. [[CrossRef](#)] [[PubMed](#)]
- Miličić, S. Box-counting dimensions of generalised fractal nests. *Chaos Solit. Fractals* **2018**, *113*, 125–134. [[CrossRef](#)]
- Valla, M.; Nedvěd, J.; Pavlík, D.; Adam, V.; Hubálek, J.; Trnková, L.; Kizek, R.; Provazník, I. Box Counting Method in Record, Processing and Evaluation of Genomic Signals. *J. Biochem. Technol. Hyderabad India* **2010**, *2*, 91–93.
- Wang, S.; Zhang, J.; Feng, F.; Qian, X.; Jiang, L.; Huang, J.; Liu, B.; Li, J.; Xia, Y.; Feng, P. Fractal analysis on artificial profiles and electroencephalography signals by roughness scaling extraction algorithm. *IEEE Access* **2019**, *7*, 89265–89277. [[CrossRef](#)]
- Zhou, G.; Wang, X.; Feng, F.; Feng, P.; Zhang, M. Calculation of fractal dimension based on artificial neural network and its application for machined surfaces. *Fractals* **2021**, *29*, 2150129–2151936. [[CrossRef](#)]
- Li, Z.; Qian, X.; Feng, F.; Qu, T.; Xia, Y.; Zhou, W. A continuous variation of roughness scaling characteristics across fractal and non-fractal profiles. *Fractals* **2021**, *29*, 2150109–2150638. [[CrossRef](#)]
- Majumdar, A.; Tien, C. Fractal characterization and simulation of rough surfaces. *Wear* **1990**, *136*, 313–327. [[CrossRef](#)]
- Berry, M.V.; Lewis, Z.; Nye, J.F. On the weierstrass-mandelbrot fractal function. *Proc. R. Soc. Lond. A Math. Phys. Sci.* **1980**, *370*, 459–484.

32. Zou, M.; Yu, B.; Feng, Y.; Xu, P. A monte carlo method for simulating fractal surfaces. *Phys. A Stat. Mech. Its Appl.* **2007**, *386*, 176–186. [[CrossRef](#)]
33. Takagi, T. A simple example of the continuous function without derivative. *Collect. Pap. Teiji Takagi* **1973**, *1*, 5–6.
34. Falconer, K. *Fractal Geometry: Mathematical Foundations and Applications*; John Wiley & Sons: Hoboken, NJ, USA, 2004.
35. Chen, Z.; Liu, Y.; Zhou, P. A comparative study of fractal dimension calculation methods for rough surface profiles. *Chaos Solit. Fractals* **2018**, *112*, 24–30. [[CrossRef](#)]
36. Zuo, X.; Tang, X.; Zhou, Y. Influence of sampling length on estimated fractal dimension of surface profile. *Chaos Solit. Fractals* **2020**, *135*, 109755. [[CrossRef](#)]
37. Yao, K.; Chen, H.; Peng, W.; Wang, Z.; Yao, J.; Wu, Y. A new method on box dimension of weyl-marchaud fractional derivative of weierstrass function. *Chaos Solit. Fractals* **2021**, *142*, 110317. [[CrossRef](#)]
38. Kulesza, S.; Bramowicz, M. A comparative study of correlation methods for determination of fractal parameters in surface characterization. *Appl. Surf. Sci.* **2014**, *293*, 196–201. [[CrossRef](#)]
39. Liu, Y.; Wang, Y.; Chen, X.; Yu, H. A spherical conformal contact model considering frictional and microscopic factors based on fractal theory. *Chaos Solit. Fractals* **2018**, *111*, 96–107. [[CrossRef](#)]
40. Mohammadi, Y.; Ahmadi, K. Frequency domain analysis of regenerative chatter in machine tools with linear time periodic dynamics. *Mech. Syst. Signal Process.* **2019**, *120*, 378–391. [[CrossRef](#)]
41. Niu, J.; Jia, J.; Wang, R.; Xu, J.; Sun, Y.; Guo, D. State dependent regenerative stability and surface location error in peripheral milling of thin-walled parts. *Int. J. Mech. Sci.* **2021**, *196*, 106294. [[CrossRef](#)]
42. Rafal, R.; Pawel, L.; Krzysztof, K.; Bogdan, K.; Jerzy, W. Chatter identification methods on the basis of time series measured during titanium superalloy milling. *Int. J. Mech. Sci.* **2015**, *99*, 196–207. [[CrossRef](#)]
43. Aslan, D.; Altintas, Y. On-line chatter detection in milling using drive motor current commands extracted from cnc. *Int. J. Mach. Tools Manuf.* **2018**, *132*, 64–80. [[CrossRef](#)]
44. Ragab, A.; Yacout, S.; Ouali, M.-S.; Osman, H. Prognostics of multiple failure modes in rotating machinery using a pattern-based classifier and cumulative incidence functions. *J. Intell. Manuf.* **2019**, *30*, 255–274. [[CrossRef](#)]
45. Li, X.; Guan, X. Time-frequency-analysis-based minor cutting edge fracture detection during end milling. *Mech. Syst. Signal Process.* **2004**, *18*, 1485–1496. [[CrossRef](#)]
46. Cao, H.; Yue, Y.; Chen, X.; Zhang, X. Chatter detection in milling process based on synchrosqueezing transform of sound signals. *Int. J. Adv. Manuf. Technol.* **2017**, *89*, 2747–2755. [[CrossRef](#)]
47. Liu, C.; Zhu, L.; Ni, C. The chatter identification in end milling based on combining emd and wpd. *Int. J. Adv. Manuf.* **2017**, *91*, 3339–3348. [[CrossRef](#)]
48. Cuka, B.; Kim, D.-W. Fuzzy logic based tool condition monitoring for end-milling. *Robot. Comput.-Integr. Manuf.* **2017**, *47*, 22–36. [[CrossRef](#)]
49. Elangovan, M.; Sugumaran, V.; Ramachandran, K.; Ravikumar, S. Effect of svm kernel functions on classification of vibration signals of a single point cutting tool. *Expert Syst. Appl.* **2011**, *38*, 15202–15207. [[CrossRef](#)]
50. Elshorbagy, A.; Simonovic, S.; Panu, U. Noise reduction in chaotic hydrologic time series: Facts and doubts. *J. Hydrol.* **2002**, *256*, 147–165. [[CrossRef](#)]
51. Altintas, Y.; Budak, E. Analytical prediction of stability lobes in milling. *CIRP Ann.* **1995**, *44*, 357–362. [[CrossRef](#)]
52. Jensen, S.; Shin, Y.C. *Stability Analysis in Face Milling Operations, Part 1: Theory of Stability Lobe Prediction*; ASME: New York, NY, USA, 1999.
53. Pour, M.; Torabizadeh, M.A. Improved prediction of stability lobes in milling process using time series analysis. *J. Intell. Manuf.* **2016**, *27*, 665–677. [[CrossRef](#)]